ACS Catalysis

pubs.acs.org/acscatalysis Research Article

Enhanced Catalytic Performance through In Situ Encapsulation of Ultrafine Ru Clusters within a High-Aluminum Zeolite

Jiangqian Yang,[▽] Ying He,[▽] Jiang He, Yuanshuai Liu, Huawei Geng, Shaohua Chen, Lu Lin, Meng Liu, Tiehong Chen, Qike Jiang, Bert M. Weckhuysen,* Wenhao Luo,* and Zhijie Wu*

Cite This: *ACS Catal.* 2022, 12, 1847−1856 Read Online

ACCESS | Metrics & More | Article Recommendations | Supporting Information

ABSTRACT: Zeolite-encapsulated metal clusters have been shown to be an effective bifunctional catalyst for tandem catalysis. Nevertheless, the efficient encapsulation of nanometric metal species into a high-aluminum ZSM-5 zeolite still poses a significant challenge. In this contribution, we have prepared well-dispersed and ultra-small Ru clusters encapsulated within a high-aluminum ZSM-5 zeolite (with a Si/Al ratio of ∼30−40) via an in situ two-stage hydrothermal synthesis method. Small Ru clusters with an average size of ∼1 nm have been identified by scanning transmission electron microscopy and hydrogen chemisorption. Shape-selective hydrogenation experiments with different probe molecules reveal a predominant encapsulation (∼90%) of metal clusters within the MFI zeolite cavities, which significantly enhances thermal stability of metal clusters against sintering. ^{27}Al magic angle spinning nuclear magnetic resonance and Brønsted acid site (BAS) titration experiments show the successful incorporation of aluminum species (>99%) into the zeolite framework and build-up of intimacy between the Ru clusters and BASs at a sub-nanometric level. The resulting Ru@H-ZSM-5 shows an enhanced activity and stability for the crucial hydrodeoxygenation (HDO) of phenol to cyclohexane, in biomass valorization. This synthesis strategy could be of great help for the rational design and development of zeolitic bifunctional catalysts and could be extended to other crystalline porous materials.

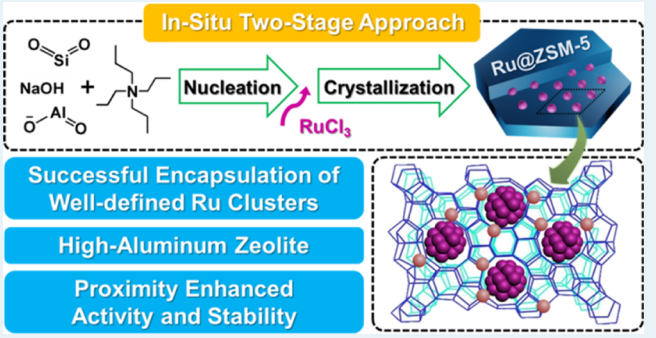

KEYWORDS: *encapsulation, metal clusters, high-aluminum zeolite, stability, hydrodeoxygenation*

1. INTRODUCTION

The encapsulation of metal clusters within zeolite micropores or cavities is an attractive and efficient strategy for the preparation of ultrafine metal nanoparticles. The confined environment of zeolites could provide the spatial restriction for the small metal entities, which can improve the metal stability against sintering and leaching of active metal species during catalysis.[1,2] Additionally, such a successful encapsulation can afford site proximity between metal and acid sites, which could improve catalytic performance owing to providing synergistic effects between the different functional sites.[3−12] The impregnation and ion-exchange methods are traditional approaches widely employed for achieving metal species highly dispersed into zeolite cavities.[1−5] However, both methods have their own limits and are either not suitable or effective for the metal encapsulation into small-pore zeolites (8-member ring zeolite, e g., LTA zeolite, 0.42 nm in aperture size) and medium-pore zeolites (10-member ring zeolite, e g., MFI zeolite, 0.55 nm in aperture size).[13] Notably, previous studies have shown some successful examples of metal encapsulation into MFI zeolites via different approaches.[14−30] However, most MFI zeolites in those cases were related with purely siliceous MFI zeolites (silicate-1) and TS-1. Recently, a seed-assistant hydrothermal method has been reported for the synthesis of ZSM-5 zeolite-encapsulated metal or metal oxide.[17] Such an approach requires a hierarchical ZSM-5 zeolite as the seed, allowing the entrance of metal precursors into mesopores via impregnation, and the preloaded metal precursors could be encapsulated subsequently during the following hydrothermal crystallization.[17,29] Xu et al. developed a one-pot encapsulation method via steam-assisted crystallization (one of the typical dry-gel conversion methods in zeolite synthesis) to encapsulate Pt clusters within the ZSM-5 zeolite with a Si/Al ratio of ∼60.[18] Still, more effort needs to be devoted to overcoming the severe mass and heat transfer problems in this approach for the further practical application. Particularly, the encapsulation of ultrafine metal clusters within a high-aluminum ZSM-5 zeolite

Received: November 1, 2021
Revised: January 3, 2022
Published: January 19, 2022

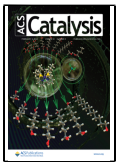

https://doi.org/10.1021/acscatal.1c05012
ACS Catal. 2022, 12, 1847−1856

(i.e., a framework Si/Al ratio of <50 for the MFI zeolite) is limitedly reported, which is one of the most important bifunctional materials from both fundamental and practical perspectives. Still, the successful encapsulation of metal clusters into a high-aluminum ZSM-5 zeolite encompasses several challenges with respect to the following: (1) the failure in the formation of the MFI structure as the presence of metal precursors may interrupt the assembly of MFI zeolite units; (2) the failure of metal encapsulation as the premature precipitation of metal precursors can occur before zeolite ZSM-5 crystallization; and (3) the unsuccessful incorporation of Al species into the zeolite framework.

Tandem catalysis is an effective strategy for chemical processes with multiple consecutive reaction steps because it could circumvent costly and energy-intensive steps of separation and purification.[31,32] Different functional sites with exquisite architectures are often required by such tandem catalysis to enable the efficient coupling of consecutive reactions.[33] The intimacy between metal and acid sites within the cavities of zeolites could provide advances in activity and selectivity in such tandem catalysis.[31,34] Hydrodeoxygenation (HDO) of biomass-derived phenol into the transportation fuel-range hydrocarbons is one of the essential reactions in lignin valorization, which addresses an on-going attention owing to its increasing availability at low cost.[35,36] Different HDO pathways of phenol have been proposed, including (i) hydrogenation/dehydration, (ii) direct deoxygenation (DDO), and (iii) tautomerization.[37−39] In the aqueous phase, bifunctionally catalyzed phenol HDO followed a route consisting of four steps: phenol is first hydrogenated to cyclohexanone followed by hydrogenation of cyclohexanone into cyclohexanol, and then, cyclohexanol is dehydrated to cyclohexene, and finally, the hydrogenation of cyclohexene into cyclohexane occurs.[38−42] In this cascade HDO path, metal sites catalyze hydrogenation reactions, and acid sites catalyze dehydration.[37−39] As versatile solid acids, zeolites with their unique shape selectivity, robust hydrothermal stability, and controllable acidity have been extensively applied in designing bifunctional materials by inclusion of redox-active metal moieties. Close proximity between metal and acid sites inside the cavities of zeolites provides additional benefits such as shortening the diffusion path, improving metal stability, and sometimes even delivering synergistic effects in catalysis.[36,43,44]

Herein, well-dispersed and ultrafine Ru clusters (∼1 nm) encapsulated in the cavities of a high-aluminum ZSM-5 zeolite have been developed by an in situ hydrothermal synthesis strategy, which involves two separate steps: zeolite nucleation and metal encapsulation during crystallization. The successful metal encapsulation of the resulting Ru@ZSM-5 catalyst has been validated by scanning transmission electron microscopy (STEM) and controlled hydrogenation experiments with two probe molecules (i.e., toluene and 1,3,5-triisopropylbenzene).[45,46] Thermal-treatment experiments show an excellent thermal stability of Ru@ZSM-5, with no apparent sintering observed up to 873 K. ^{27}Al magic angle spinning (MAS) nuclear magnetic resonance (NMR) confirms the successful incorporation of Al species into the zeolite framework. Finally, a metal-acid proximity can be built over the Ru@H-ZSM-5 via a further ion-exchange treatment of Ru@ZSM-5. The obtained Ru@H-ZSM-5 possesses enhanced catalytic performance in the HDO of phenol, which extends the notion of "the closer, the better" into biomass catalysis. This efficient synthesis approach for metal clusters encapsulated within zeolite-based materials may open new perspectives for the rational design of bifunctional catalysts for tandem catalysis.

2. RESULTS AND DISCUSSION

2.1. Synthetic Strategy for Encapsulation of Ru Clusters. Scheme 1 shows the in situ encapsulation strategy

Scheme 1. Schematic Illustration of the In Situ Two-Stage Hydrothermal Synthesis Approach for the Encapsulation of Metal Clusters Into a High-Aluminum ZSM-5

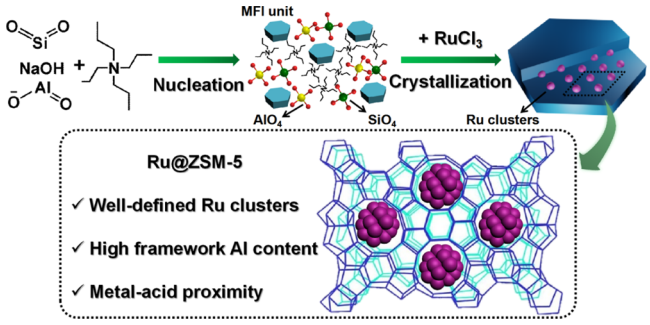

for the synthesis of Ru@ZSM-5, in which the metal encapsulation is realized by a two-step process: the nucleation of MFI structure units at a temperature of 373 K and crystallization at a relatively high temperature of 443 K. Such a two-step process is necessary for the successful encapsulation of metal clusters into the high-aluminum ZSM-5 zeolites. If a one-step hydrothermal process is applied for the metal encapsulation into ZSM-5, the high pH conditions applied for the nucleation and crystallization of the MFI zeolite could result in metal precipitation quickly and further lead to a failure of metal encapsulation. Iglesia et al. confirmed that the high pH and temperature conditions (pH = 12, >433 K) favoring fast nucleation and crystallization of MFI could lead to the formation of bulk metal (Ru or Pt) hydroxide precipitates during the direct hydrothermal process.[14] Comparing to the synthesis of a high-silica ZSM-5 zeolite, more organic templates as the structure direction agents are required for the synthesis of a high-aluminum ZSM-5. The addition of a metal precursor during the nucleation step can interrupt the assembly of a zeolite, owing to the strong coordination between metal species and organic templates. Therefore, a separate preliminary nucleation step is crucial to realize the metal encapsulation during the crystallization step, which can suppress the formation of bulk precipitates from the metal species and efficiently prevent the negative impact of the metal precursor on the assembly of the zeolite under the hydrothermal conditions (Figures S1 and S2).

In the proposed in situ two-stage process, the nucleation of ZSM-5 proceeds in a starting alumino-silicate gel with a high SiO_2/H_2O weight ratio of 0.42 (a supersaturated solution) at 373 K, to facilitate the formation of a significant amount of nano-sized zeolite crystals, in agreement with the reported results that a high concentration of solid gel enables the formation of a significant amount of zeolite nano-crystals.[45] The subsequent introduction of $RuCl_3$ solution into the zeolite nucleus solution can avoid the formation of bulk hydroxide precipitates during crystallization, enabling a homogeneous distribution of Ru species encapsulated inside the ZSM-5. Analogically, successful encapsulation of metal clusters within inorganic materials via a two-step synthesis approach has been

https://doi.org/10.1021/acscatal.1c05012
ACS Catal. 2022, 12, 1847−1856

achieved by Wang et al. recently.[47] For comparison, Ru/ZSM-5-HT via a direct hydrothermal crystallization of the $RuCl_3$-containing MFI gels and Ru/ZSM-5-IP via wet impregnation of ZSM-5 with a $RuCl_3$ solution were also prepared.

2.2. Physicochemical Characterizations of Different Catalyst Materials. The X-ray diffraction (XRD) patterns of Ru/ZSM-5-IP, Ru/ZSM-5-HT, and Ru@ZSM-5 show characteristic peaks of the MFI structure (JCPDS no.: 49-0657) (Figure 1). The absence of characteristic peaks corresponding to Ru metal or oxide crystal indicates no formation of large Ru particles in the as-synthesized samples. Notably, Ru@ZSM-5 shows a relatively high crystallinity of MFI, indicating that the assembly of MFI zeolite units was not interrupted upon metal addition. The chemical composition, metal dispersion, and texture properties of different samples are listed in Table 1. The inductively coupled plasma-atomic emission spectroscopy (ICP-AES) results show that all zeolite samples have a similar Si/Al ratio in a range from 33 to 38, indicating a similar Al content in all ZSM-5 zeolites. Compared with parent ZSM-5, Ru/ZSM-5-IP shows no apparent change in porosity but only a decrease in micropore volume from 0.13 to 0.11 cm^3/g (Table 1). Combining with a decrease in zeolite crystallinity for the Ru/ZSM-5-IP observed in XRD, this drop in micropore volume might be originated from the partial collapse of the zeolite structure during metal impregnation steps (calcination and reduction processes). Ru/ZSM-5-HT shows a slight decrease in the mesopore porosity and surface area, probably owing to an increase in zeolite crystal size (Figure S3) and zeolite crystallinity. Ru@ZSM-5 shows a similar mesopore porosity and surface area as those of Ru/ZSM-5-HT but with the most decrease in the micropore porosity and surface area (Table 1 and Figure S4), suggesting the successful encapsulation of Ru species into zeolite cavities. Moreover, compared with other samples (Ru/ZSM-5-HT, Ru/ZSM-5-IP, and ZSM-5), a slightly higher zeolite crystallinity is indicated for the Ru@ZSM-5 by XRD (Figure 1 and Table 1), suggesting a better zeolite crystallinity structure of the Ru@ZSM-5 via the in situ two-stage encapsulation approach.

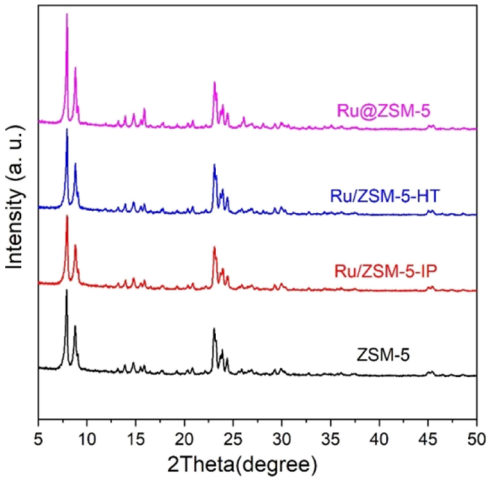

Figure 1. XRD patterns of the different Ru-containing ZSM-5 zeolites and parent ZSM-5.

STEM and the corresponding energy-dispersive X-ray (EDX) spectroscopy were employed to further study the structural properties of Ru metal particles in different samples (Figures 2, S5 and S6). Random Ru particles that ranged from 1−30 nm could be distinguishable over Ru/ZSM-5-IP and Ru/ZSM-5-HT, prepared by the impregnation and one-step hydrothermal method separately (Figure 2a,b). Analysis of STEM images shows an average Ru particle size of 11.5 nm for Ru/ZSM-5-IP and 7.5 nm for Ru/ZSM-5-HT, in which Ru particles are mainly located at the external surface of the ZSM-5 zeolite. In contrast, Ru@ZSM-5 shows no apparent large Ru particles on the external surface of the zeolite (Figure 2c), and Ru species can be visualized in the high-magnification STEM image, with an average particle diameter of about 1.3 nm inside the ZSM-5 crystal. H_2 chemisorption results (Table 1) further confirm well-defined Ru particles of ∼1.4 nm in Ru@ZSM-5, with a metal dispersion of ∼80%. EDX-mapping analysis (Figures 2e and S5) points to a homogeneous distribution of Ru clusters in the Ru@ZSM-5. Therefore, the in situ two-stage encapsulation strategy shows significant advantages in the formation of highly dispersed Ru clusters, compared to the traditional wet impregnation method and the direct hydrothermal method.

When metal species are encapsulated inside the zeolite during the in situ two-stage metal encapsulation approaches (Ru@ZSM-5), the full removal of the N-containing template (i.e., TPABr) during calcination and reduction steps may be challenging owing to the strong coordination of the residual organic template species on the metal surface, which could

Table 1. Physicochemical Properties of Different Ru-Containing Zeolites and Materials

						BET surface area (m^2/g)[e]			volume (cm^3/g)[e]		
Samples	relative crystallinity (%)[a]	Si/Al ratio[b]	Ru loading (wt %)[b]	D[c]	d_{chem} (nm)[d]	micro-pore	meso-pore	total	micro-pore	meso-pore	total
ZSM-5	100	33.5				228	112	340	0.13	0.15	0.28
Ru/ZSM-5-IP	93	34.8	0.46	0.22	4.9	231	101	332	0.11	0.16	0.27
Ru/ZSM-5-HT	107	37.1	0.15	0.18	6.0	256	86	342	0.12	0.11	0.23
Ru@ZSM-5	112	37.5	0.53	0.79	1.4	240	86	326	0.11	0.11	0.22
Ru/H-ZSM-5-IP	87	35.2	0.48	0.24	4.6	229	96	325	0.11	0.15	0.26
Ru@H-ZSM-5	109	37.1	0.55	0.81	1.4	237	91	328	0.11	0.11	0.22
spent Ru@H-ZSM-5[f]	106	36.5	0.50	0.76	1.4	217	92	309	0.09	0.10	0.19
Ru/SiO_2			0.51	0.68	1.6	103	242	345	0.04	0.48	0.52

[a]Determined by XRD analysis. [b]Determined by ICP-AES analysis. [c]Metal dispersion determined by H_2 chemisorption.[46] [d]Mean particle diameter determined by H_2 chemisorption.[46] [e]Specific surface area obtained by the BET method; Micropore surface area and micropore volume calculated by the t-plot method; Mesopore volume calculated by subtracting the micropore volume from the total volume. [f]The spent Ru@ZSM-5 zeolite is obtained after four consecutive runs of phenol HDO.

https://doi.org/10.1021/acscatal.1c05012
ACS Catal. 2022, 12, 1847−1856

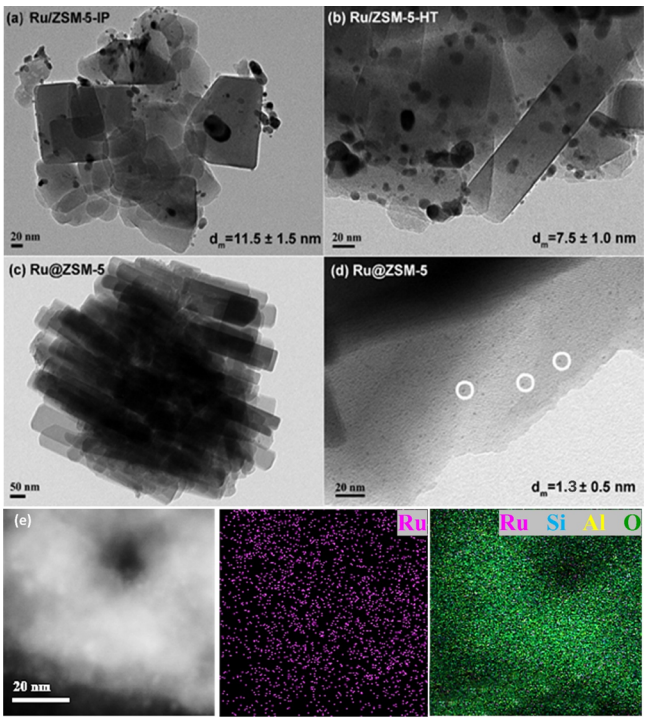

Figure 2. STEM images and the corresponding average diameters of Ru particles (d_m derived from measurements of over 200 particles) of (a) Ru/ZSM-5-IP, (b) Ru/ZSM-5-HT, and (c,d) Ru@ZSM-5. (e) EDX spectral imaging of the Ru@ZSM-5 and corresponding elemental maps: Ru pink, Si blue, Al yellow, and O green, showing that Ru species are highly dispersed inside the zeolite ZSM-5.

block the access to the active sites and thus bring negative impacts on catalytic performance. The surface cleanliness index (CI), defined as the ratio of d_{chem} (determined by H_2 chemisorption in Table 1) to d_m (obtained from STEM in Figure 2), can be an important descriptor for the removal extent of residual fragments.[14,46] The Ru@ZSM-5 shows a CI value of 1.08. This near-unity value indicates a complete removal of the organic template, which points to an essentially clean surface for metal species in the Ru@ZSM-5. This in situ two-stage approach not only achieves successful metal encapsulation but also affords good accessibility to the encapsulated metal species.

2.3. Validation of Metal Encapsulation. The small apertures of the MFI zeolite allow them to sieve reactants and products based on their molecular size. To further quantify the fraction of the Ru clusters encapsulated inside the zeolite cavities, hydrogenation tests with two probing molecules , toluene (kinetic diameter: 0.55 nm, accessible into the cavities of MFI) and 1,3,5-triisopropylbenzene (TIPB, kinetic diameter: 0.85 nm, inaccessible into the cavities of FAU), with different sizes have been performed.[48] To suppress Brønsted acid site (BAS)-induced side reactions (i.e., TIPB dealkylation and toluene disproportionation), the BAS of all samples was further removed by an ion-exchange treatment with sodium cations (Na^+) before the hydrogenation tests. The analysis of Fourier transform-infrared spectroscopy (FT-IR) of pyridine adsorption confirms the removal of all the BASs in these samples (Figure S7). Ru/SiO_2 is used as the benchmark catalyst with all the Ru particles located outside of the support for the hydrogenation tests. The extent of encapsulation specificity can be reflected by a ratio of turnover frequency (TOF) values of two different probe molecules during hydrogenation (Table 2). For example, the higher χ and φ values provide more rigorous evidence for the dominance of metal clusters encapsulated inside the spatially constrained zeolite cavities. n represents the fraction of Ru species located inside the zeolite.

Table 2. Catalytic Performances of Ru Metal Supported on ZSM-5 Zeolites and SiO_2 in Hydrogenation of Aromatics[a]

	TOF (s^{-1})				
Catalysts	toluene hydrogenation	TIPB hydrogenation	χ[b]	φ[c]	n[d]
Ru/ZSM-5-IP	0.84	0.65	1.3	1.6	0.23
Ru/ZSM-5-HT	0.85	0.52	1.6	2.0	0.39
Ru@ZSM-5	0.71	0.06	11.8	14.8	0.92
Ru/SiO_2	0.82	1.02	0.8		

[a]Reaction conditions: 111 kPa toluene or 6.8 kPa TIPB, 2.75 MPa H_2, and 423 K. The zeolite samples were treated by the Na^+ cation ion exchange to remove the acid sites of samples. [b]$\chi = TOF_{toluene}/TOF_{TIPB}$. [c]$\varphi = \chi_{zeolite}/\chi_{SiO2}$. [d]$n = (TOF_{toluene} - TOF_{TIPB})/TOF_{toluene}$. If we regard $TOF_{toluene}$ as all the Ru clusters on the zeolite and TOF_{TIPB} as the Ru clusters at the surface of the zeolite, then n represents the fraction of Ru located in the micropores of zeolites.

Compared with the $TOF_{toluene}$ of 0.82 s^{-1} for Ru/SiO_2, similar $TOF_{toluene}$ values were observed for Ru/ZSM-5-HT and Ru/ZSM-5-IP in toluene hydrogenation, while only a slight decrease in $TOF_{toluene}$ to 0.71 s^{-1} was observed for Ru@ZSM-5. Notably, Ru@ZSM-5 exhibited the highest χ and φ values (χ = 11.8 and φ = 14.8) among all catalysts. The fraction of Ru clusters inside the zeolite cavities could be further determined to be 92% for Ru@ZSM-5, which is much higher than the values of 39% for Ru/ZSM-5-HT and 23% for Ru/ZSM-5-IP. These results are again in good line with STEM and chemisorption results, which confirm the predominance of Ru clusters encapsulated inside the zeolite ZSM-5 by this in situ two-stage hydrothermal synthesis method. Indeed, the proposed two-step approach holds more significant advantages in control synthesis of encapsulated metal clusters inside the zeolite, compared to the direct hydrothermal method and traditional wet impregnation method.

The confined environment of the zeolite could provide the spatial restriction for metal clusters, which thus enhances thermostability against metal agglomeration or sintering even at high temperatures. To validate the beneficial effect of metal encapsulation on thermostability, we have compared the average Ru particle size of Ru@ZSM-5 with that of Ru/SiO_2 without the metal-encapsulated structure after thermo treatments at a set of variated temperatures. Notably, Ru clusters in Ru@ZSM-5 show no apparent change (stable at ~ 1.5 nm) in the average Ru diameters even up to a high treatment temperature of 873 K (Figure 3), indicating no apparent occurrence of metal agglomeration or sintering under thermo treatments. The excellent thermostability of Ru@ZSM-5 is mainly attributed to the effective isolation of Ru species by their spatially uniform distribution and confinement throughout ZSM-5 crystals. In contrast, Ru/SiO_2 shows a linear increase in the metal particle diameter from 1.6 to 2.7 nm, when it was treated at a variated temperature from 573 to 873 K. These results further prove that metal encapsulation significantly promotes thermostability of metal species against metal agglomeration/sintering.

https://doi.org/10.1021/acscatal.1c05012
ACS Catal. 2022, 12, 1847−1856

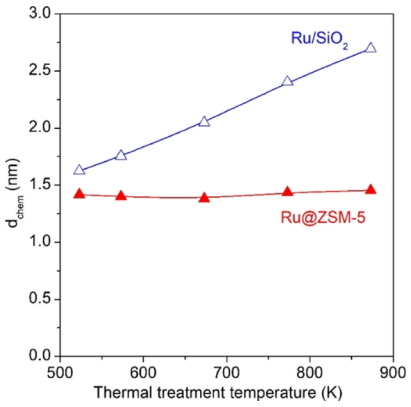

Figure 3. Average diameters of Ru species in Ru@ZSM-5 and Ru/SiO_2 after thermal treatment under a N_2 flow of 120 mL/min at a set of variated temperatures from 573 to 873 K. The Ru particle diameters were determined by H_2 chemisorption.

2.4. Construction of Metal-Acid Intimacy. The successful encapsulation of metal clusters enables us to construct a close proximity of metal and acid sites inside the cavities of the zeolite, which may afford additional benefits and sometimes synergistic effects in catalysis.[5,10,32,49] Zeolite-tailored site proximity in the constrained environment has shown to boost the hydrodeoxygenation performance in biomass valorization.[48] In view of this, H-type zeolites (H-ZSM-5, Ru/H-ZSM-5-IP, and Ru@H-ZSM-5) are further prepared after an ion exchange of self-prepared samples (ZSM-5, Ru/ZSM-5-IP, and Ru@ZSM-5) with a NH_4Cl solution, followed by subsequent calcination and reduction processes. The results of NH_3-TPD showed that the total acid sites (0.45−0.51 mmol/g acid sites) and acid strength of all samples were similar (Figure S8). Additionally, ^{27}Al MAS NMR has been employed for a detailed comparison of the aluminum speciation of the parent H-ZSM-5, Ru/H-ZSM-5-IP, and Ru@H-ZSM-5. Different coordination states of Al species [Al(IV), Al(V), and Al(VI) species] can be discriminated, and the relative portion of each species can be further quantified, as shown in Figure 4.[50−52] For the parent H-ZSM-5, a primary resonance of Al(IV) (54.9 ppm, 96.3%) represents tetrahedral framework aluminum (FAL) species, while a minor of Al(VI)

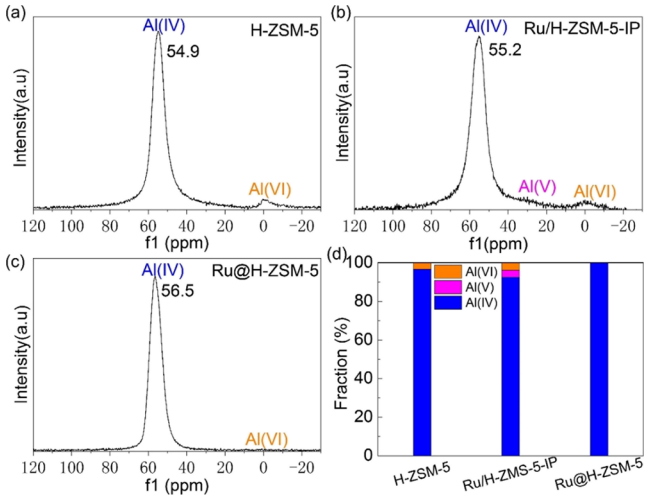

Figure 4. ^{27}Al MAS NMR spectra of H-ZSM-5, Ru/H-ZSM-5-IP, and Ru@H-ZSM-5.

(around 0 ppm, 3.7%) can be assigned to octahedral extra-framework aluminum (EFAL) species, originating from the slight dealumination during synthesis. For the Ru/H-ZSM-5-IP, the Al(IV) resonance (55.2 ppm, 93.3%) shows a shift of the signal to higher resonance and an increased horizontal broadening compared to that for the as-synthesized H-ZSM-5. This is typically attributed to the influence of adjacent cationic species, either by Ru or EFAL species.[52] Indeed, Ru deposition by impregnation results in an increase in EFAL species [Al(V): 2.4% and Al(VI): 4.3%] compared to the parent H-ZSM-5. Combining with the average Ru particle size of 4.9 nm in Ru/H-ZSM-5-IP, Ru species are unlikely to provide this strong perturbation in the zeolite channels. Therefore, it is highly rational that EFAL species in the MFI pores interact with the FAL and cause this shift and the broadening of the Al(IV) signal. Notably, a narrow and significant Al(IV) signal (99.2%), with an isotropic shift of 56.5 ppm, and a marginal Al(VI) signal (0.8%) are shown for Ru@H-ZSM-5, indicating the predominance of Al species located in the FAL. Based on the results of trace EFAL species and highly dispersed (~1 nm) Ru ultrafine clusters in the zeolite cavities, the observed upshift of Al(IV) for Ru@H-ZSM-5 compared to that for the parent H-ZSM-5 should mainly originate from the interaction between FAL and the adjacent Ru clusters in Ru@H-ZSM-5. No obvious broadening or distortion of the Al(IV) signal of Ru@H-ZSM-5 confirms the homogeneous dispersion of Ru clusters and the limit amount of EFAL. Thus, our proposed in situ two-stage synthetic strategy is efficient not only for incorporating Al species into the zeolite FAL but also for metal encapsulation inside the zeolite affording a close metal-acid proximity.

The BAS distribution (on the external surface or inside zeolite cavities) in different zeolite materials has been determined by the probe reaction of methanol dehydration tests with titration of triphenylphosphine.[45,49] The portion of the BAS on the external surface or in zeolite cavities in different zeolite samples could be determined and is listed in Table 3. For the H-ZSM-5 zeolite, the BAS proportion can

Table 3. BAS Distribution in Different Zeolites by Titration Experiments

sample	Brønsted acid amount (mmol/g)		F_{ext} (%)[a]	F_{cav} (%)[b]
	on external surface	inside cavities		
H-ZSM-5	0.05	0.25	17	83
Ru/H-ZSM-5-IP	0.02	0.18	10	90
Ru@H-ZSM-5	0.005	0.16	3	97
Ru/SiO_2 + H-ZSM-5	0.05	0.24	17	83
Spent Ru@H-ZSM-5[c]	0.002	0.11	2	98

[a]Fraction of the external BAS calculated by TPP titration. [b]Fraction of the BAS within the zeolite cavity, which can be obtained as 1-F_{ext}%. [c]The spent Ru@ZSM-5 after four consecutive runs in the HDO of phenol.

achieve 17% on the external surface and 83% in zeolite cavities. For Ru/H-ZSM-5-IP, the BAS fraction on the external surface decreases to 10%, and the internal BAS fraction is 90% after Ru addition. For Ru@H-ZSM-5, the BAS fraction in zeolite cavities can achieve up to 97%, in line with the high zeolite crystallinity and good incorporation of Al species into FAL (>99%). Combined with the 92% of Ru species inside the zeolite cavities by hydrogenation tests (Table 2), a close

https://doi.org/10.1021/acscatal.1c05012
ACS Catal. 2022, 12, 1847−1856

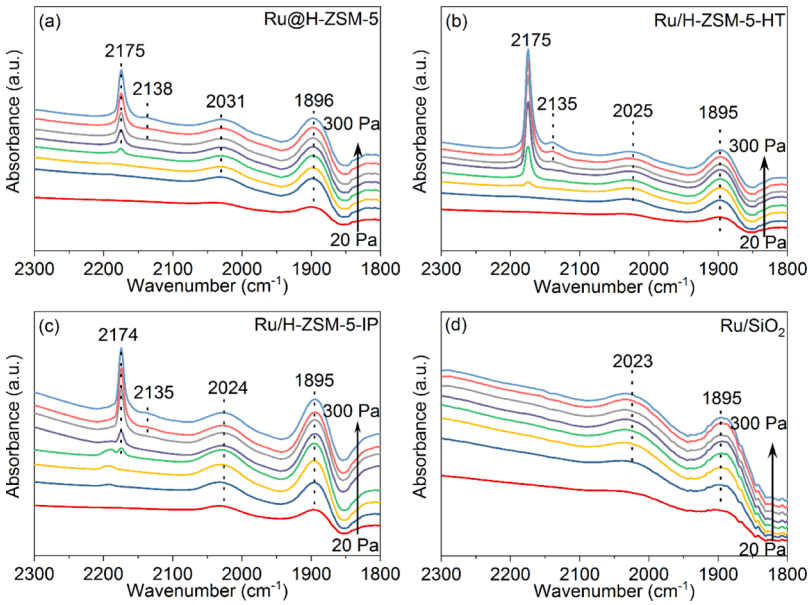

Figure 5. FT-IR spectra of CO adsorbed on (a) Ru@H-ZSM-5, (b) Ru/H-ZSM-5-HT, (c) Ru/H-ZSM-5-IP, and (d) Ru/SiO_2 at 103 K and different pressures.

proximity between Ru clusters and the acid sites within the zeolite cavities is verified in Ru@H-ZSM-5.

The FT-IR spectra of Ru@H-ZSM-5, Ru/H-ZSM-5-HT, Ru/H-ZSM-5-IP, and Ru/SiO_2 after CO adsorption are shown in Figure 5. All the three zeolite samples show the development of signals at about 2174, 2135, 2024, and 1895 cm^{-1}, corresponding to CO adsorbed on the protons of the zeolite, multi-coordinated Ru^{n+}−CO, linear Ru−CO, and bridging Ru−CO species, respectively.[48,53] Notably, the blue shift of Ru^{n+}−CO (~3 cm^{-1}) and linear Ru−CO (~7 cm^{-1}) signals is observed for Ru@H-ZSM-5 comparing to that for Ru/H-ZSM-5-HT, Ru/H-ZSM-5-IP, and Ru/SiO_2. Those shifts indicate that the encapsulated Ru species exhibit a more positive charge, owing to the induced electronic interaction between the encapsulated Ru clusters and zeolite framework. Such an electronic interaction is also supported by H_2-TPR (Figure S9). Similar modulation of the electronic structure of Ru species was also observed with zeolite Y-encapsulated Ru clusters.[48]

2.5. Induced Intimacy Effect for the Hydrodeoxygenation of Phenol. Phenol HDO reactions have been performed to investigate the effect of the metal-acid intimacy after the successful Ru encapsulation into the zeolite ZSM-5. We have first performed the HDO of phenol at 423 K and 5.0 MPa H_2 in decalin as the solvent. Time profiles of the substrate and products are shown in Figure S10. Ru@H-ZSM-5 outperforms in catalytic activity of phenol conversion and cyclohexane productivity. Similar time profile patterns are observed with Ru/SiO_2 + H-ZSM-5, Ru/H-ZSM-5-HT, and Ru/H-ZSM-5-IP, and the intimate mixture of Ru/SiO_2 + H-ZSM-5 is selected as the benchmark catalyst without metal-acid intimacy. In comparison to Ru/SiO_2 + H-ZSM-5, Ru@H-ZSM-5 with a metal-acid proximity shows a higher phenol conversion at the same reaction time (Figure S10a), indicating that the metal-acid intimacy provided by the metal clusters encapsulated inside the zeolite promotes the catalyst activity in phenol HDO.

The selectivity patterns of the three selected catalysts, Ru@H-ZSM-5, the intimate mixture of Ru/SiO_2 + H-ZSM-5, and Ru/SiO_2 as the non-acidic catalysts are compared at different phenol conversion levels in Figure 6a−c. At different phenol conversion levels (~30 and 60% and a reaction time of 240 min), Ru@H-ZSM-5 affords a higher cyclohexane selectivity than Ru/SiO_2 + H-ZSM-5 and Ru/SiO_2. Ru/SiO_2 produces no apparent cyclohexane, with cyclohexanone and cyclohexanol as the major products even after a reaction time of 240 min. This points to the difficulty in removing oxygen from cyclohexanol solely over Ru metal sites without the aid of acid sites, in agreement with the work reported by Li et al.[54]

Cyclohexane is the target final product in the phenol HDO reaction, which can be obtained via the sequential hydrogenation and dehydration pathway (Scheme S1 and Table S1).[39,54−56] Time profiles of cyclohexane yield over different catalysts are depicted in Figure 6d. Similar patterns are observed with Ru/SiO_2 + H-ZSM-5, Ru/H-ZSM-5-HT, and Ru/H-ZSM-5-IP catalysts. Notably, Ru@H-ZSM-5 affords a faster cyclohexane yield compared to the other catalysts. Cyclohexane productivity, expressed as the number of cyclohexane molecules produced per gram of metal per time, reflects the deep HDO ability of catalysts. The values of cyclohexane productivity of different catalysts can be further determined based on the time profiles (Figure 6d). Ru@H-ZSM-5 shows the highest cyclohexane productivity of 0.442 mmol g_{Ru}^{-1} s^{-1}, which is much higher than that of Ru/SiO_2 + H-ZSM-5 (0.132 mmol g_{Ru}^{-1} s^{-1}), Ru/H-ZSM-5-HT (0.191 mmol g_{Ru}^{-1} s^{-1}), Ru/H-ZSM-5-IP (0.122 mmol g_{Ru}^{-1} s^{-1}), and Ru/SiO_2 (0 mmol g_{Ru}^{-1} s^{-1}). Similarly, Ru@H-ZSM-5 also outperforms the other catalysts in activity and cyclohexane productivity without site proximity in the HDO of phenol or cyclohexanol in water (Tables S1 and S2). The essential role of the metal-acid intimacy inside the zeolite is thus confirmed for the production of cyclohexane.

The stability of Ru@H-ZSM-5 is examined by performing consecutive tests of HDO of phenol in the water phase with a more concentrated substrate (Figure 7), in which the zeolitic catalyst materials suffer more from a stability issue in biomass-related HDO reactions under hydrothermal conditions.[36] Ru@H-ZSM-5 after the reaction was filtered and then dried in a

https://doi.org/10.1021/acscatal.1c05012
ACS Catal. 2022, 12, 1847−1856

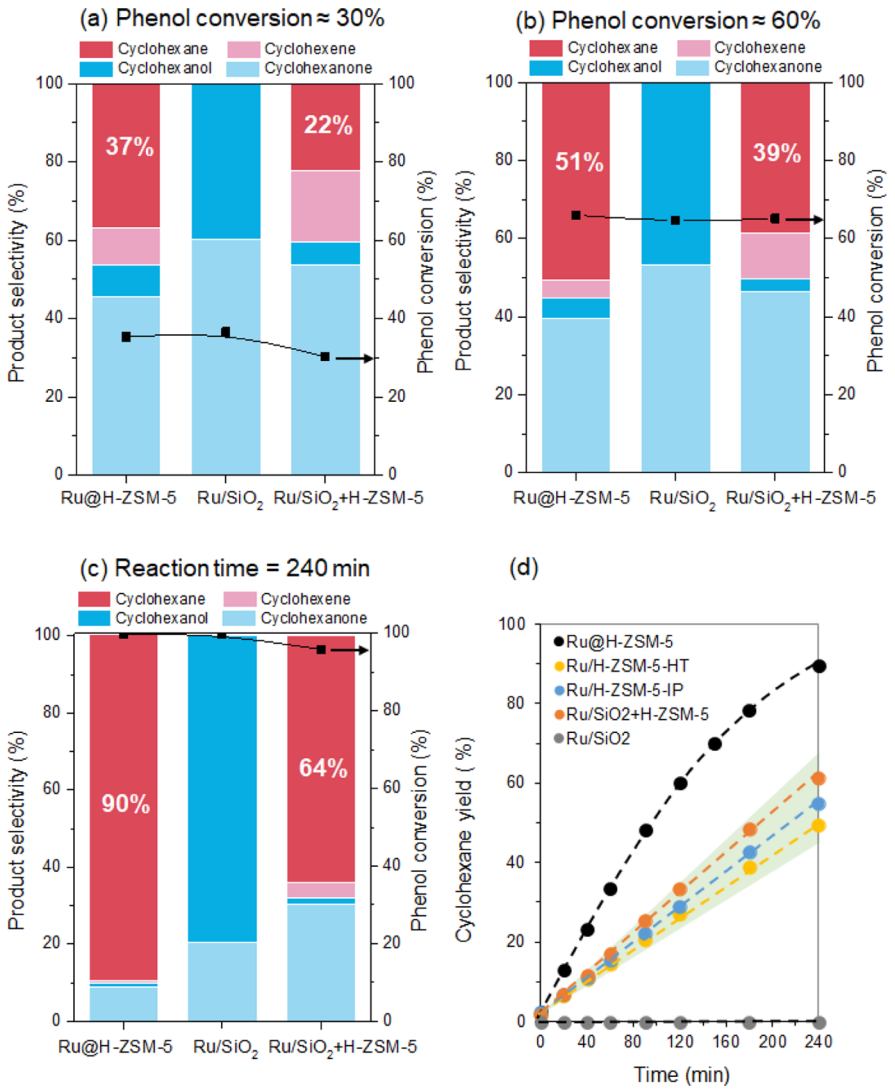

Figure 6. Selectivity comparison of Ru@H-ZSM-5, Ru/SiO_2, and Ru/SiO_2 + H-ZSM-5 at different phenol conversion levels. Phenol conversion at (a) ~30%, (b) ~60%, and (c) after 240 min of reaction time with nearly full phenol conversion. (d) Time profile of cyclohexane yield for different catalysts.

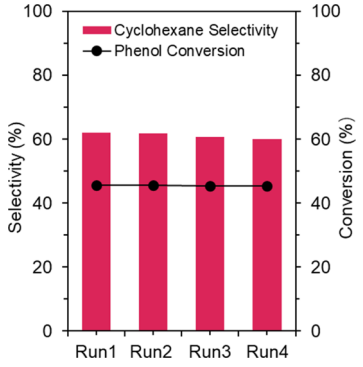

Figure 7. Recyclability of Ru@H-ZSM-5 in phenol HDO. Reaction conditions: 423 K, 5.0 MPa H_2, phenol (2.13 mmol), catalyst (200 mg), and water (10 mL).

vacuum before the next catalytic run. As shown in Figure 7, Ru@H-ZSM-5 shows no apparent drop in phenol conversion and cyclohexane selectivity, from the initial value of 45.7 to 45.4% after 4 consecutive runs. The selectivity to cyclohexane was maintained at a similar level of 60−62% upon catalysis. These marginal changes suggest an excellent stability of Ru@H-ZSM-5 with no apparent deactivation. Limited metal leaching and sintering are detected for the spent Ru@H-ZSM-5 after four consecutive runs, validating the superior stability of the Ru@H-ZSM-5 in the HDO of phenol (Table 1). No migration of the BAS is also indicated by the titration tests (Table 3), pointing to the maintenance of such intimacy, which is pivotal for catalyst stability.

Therefore, this proposed in situ two-stage hydrothermal method provides an efficient synthetic approach for the encapsulation of Ru clusters within a high-alumina ZSM-5 zeolite, which holds significant advances compared with the post synthesis method and direct hydrothermal method. The intimacy between encapsulated metal clusters and acid sites within the high-alumina zeolite enables efficiently coupling HDO reactions in the upgrading of biomass-derived phenol platform molecules, which can be further extended to other hydrotreating systems.

https://doi.org/10.1021/acscatal.1c05012
ACS Catal. 2022, 12, 1847−1856

3. CONCLUSIONS

We have successfully prepared Ru metal clusters encapsulated inside the cavities of a high-alumina ZSM-5 zeolite via an in situ two-stage synthesis method. The moderate precipitation of metal precursors synchronized with zeolite crystallization is crucial for the successful metal encapsulation. A set of advanced characterizations, combined probing tests with different probe molecules, confirms the successful encapsulation of major metal clusters (>90%) inside the zeolite cavities, together with a nearly complete aluminum incorporation into the FAL (>99%) and a high BAS fraction inside zeolite cavities (97%), providing a metal-acid intimacy inside zeolite cavities. Such intimacy in Ru@H-ZSM-5 delivers an additional benefit in activity, selectivity, and stability in the HDO of phenol. These findings provide an efficient approach for the synthesis of zeolite-based bifunctional catalysts and will be of great potential for the rational design of well-defined catalysts with proximity-boosted catalytic performance for hydrogen-assisted biomass valorizations and other energy-related transformations.

■ ASSOCIATED CONTENT

Supporting Information

The Supporting Information is available free of charge at https://pubs.acs.org/doi/10.1021/acscatal.1c05012.

Stability of RuCl3 precursors in alkaline sodium aluminate solution; XRD patterns of the RuCl3 precipitates under different hydrothermal synthesis conditions; SEM images of (a) ZSM-5, (b) Ru/ZSM-5-IP, (c) Ru/ZSM-5-HT, and (d) Ru@ZSM-5; N2 adsorption−desorption isotherms (a) and pore size distribution curves (b) of different Ru-containing ZSM-5 zeolites; corresponding EDX spectrum of Ru@ZSM-5; STEM images and the corresponding average diameters of Ru particles; pyridine-IR spectra of the different Ru-containing ZSM-5 zeolites (a) without and (b) with Na^+ ion-exchanging treatment; NH3-TPD spectra of the different Ru-containing ZSM-5 zeolite samples; H2-TPR profiles of the Ru@H-ZSM-5, Ru/H-ZSM-5-HT, and Ru/H-ZSM-5-IP samples; time profiles of phenol hydrogenation over different bifunctional catalysts in decalin; proposed reaction pathway for the hydrodeoxygenation of phenol; phenol hydrodeoxygenation over different catalysts in water; and aqueous-phase dehydration of cyclohexanol over different catalysts (PDF)

■ AUTHOR INFORMATION

Corresponding Authors

Bert M. Weckhuysen − *Inorganic Chemistry and Catalysis Group, Debye Institute for Nanomaterials Science, Utrecht University, Utrecht 3584CG, The Netherlands;* orcid.org/0000-0001-5245-1426; Email: B.M.Weckhuysen@uu.nl

Wenhao Luo − *CAS Key Laboratory of Science and Technology on Applied Catalysis, Dalian Institute of Chemical Physics, Chinese Academy of Sciences, Dalian 116023, China;* orcid.org/0000-0003-1941-3799; Email: w.luo@dicp.ac.cn

Zhijie Wu − *State Key Laboratory of Heavy Oil Processing and the Key Laboratory of Catalysis of CNPC, China University of Petroleum-Beijing, Beijing 102249, China;* orcid.org/0000-0002-8160-6615; Email: zhijiewu@cup.edu.cn

Authors

Jiangqian Yang − *State Key Laboratory of Heavy Oil Processing and the Key Laboratory of Catalysis of CNPC, China University of Petroleum-Beijing, Beijing 102249, China*

Ying He − *State Key Laboratory of Heavy Oil Processing and the Key Laboratory of Catalysis of CNPC, China University of Petroleum-Beijing, Beijing 102249, China*

Jiang He − *CAS Key Laboratory of Science and Technology on Applied Catalysis, Dalian Institute of Chemical Physics, Chinese Academy of Sciences, Dalian 116023, China; University of Chinese Academy of Sciences, Beijing 100049, China*

Yuanshuai Liu − *Inorganic Chemistry and Catalysis Group, Debye Institute for Nanomaterials Science, Utrecht University, Utrecht 3584CG, The Netherlands; Qingdao Institute of Bioenergy and Bioprocess Technology, Chinese Academy of Sciences, Qingdao 266101, China;* orcid.org/0000-0002-4020-7538

Huawei Geng − *Qingdao Institute of Bioenergy and Bioprocess Technology, Chinese Academy of Sciences, Qingdao 266101, China*

Shaohua Chen − *School of Materials Science and Engineering, Nankai University, Tianjin 300071, China*

Lu Lin − *CAS Key Laboratory of Science and Technology on Applied Catalysis, Dalian Institute of Chemical Physics, Chinese Academy of Sciences, Dalian 116023, China*

Meng Liu − *State Key Laboratory of Heavy Oil Processing and the Key Laboratory of Catalysis of CNPC, China University of Petroleum-Beijing, Beijing 102249, China*

Tiehong Chen − *School of Materials Science and Engineering, Nankai University, Tianjin 300071, China;* orcid.org/0000-0001-5162-9018

Qike Jiang − *Dalian National Laboratory for Clean Energy, Dalian Institute of Chemical Physics, Chinese Academy of Sciences, Dalian 116023, China*

Complete contact information is available at: https://pubs.acs.org/10.1021/acscatal.1c05012

Author Contributions

▽J.Y. and Y.H. contributed equally to this work.

Notes

The authors declare no competing financial interest.

■ ACKNOWLEDGMENTS

The National Key R&D Program of China (2018YFB1501602 and 2021YFA1501203), the National Natural Science Foundation of China (U1662131, 22078316, and 21721004), and the Science Foundation of the China University of Petroleum, Beijing (ZX20200125), are acknowledged for financial support.

■ REFERENCES

(1) Farrusseng, D.; Tuel, A. Perspectives on zeolite-encapsulated metal nanoparticles and their applications in catalysis. *New J. Chem.* **2016**, *40*, 3933−3949.

(2) Dai, C.; Zhang, A.; Song, C.; Guo, X. Chapter Two - Advances in the synthesis and catalysis of solid and hollow zeolite-encapsulated metal catalysts. *Adv. Catal.* **2018**, *63*, 75−115.

(3) Petrov, A. W.; Ferri, D.; Krumeich, F.; Nachtegaal, M.; van Bokhoven, J. A.; Kröcher, O. Stable complete methane oxidation over palladium based zeolite catalysts. *Nat. Commun.* **2018**, *9*, 2545.
(4) Sun, Q.; Wang, N.; Yu, J. Advances in catalytic applications of zeolite-supported metal catalysts. *Adv. Mater.* **2021**, *33*, 2104442.
(5) Chai, Y.; Shang, W.; Li, W.; Wu, G.; Dai, W.; Guan, N.; Li, L. Noble metal particles confined in zeolites: synthesis, characterization, and applications. *Adv. Sci.* **2019**, *6*, 1900299.
(6) Wu, S. M.; Yang, X. Y.; Janiak, C. Confinement effects in zeolite-confined noble metals. *Angew. Chem., Int. Ed.* **2019**, *58*, 12340−12354.
(7) Wang, L.; Wang, L.; Meng, X.; Xiao, F. S. New strategies for the preparation of sinter-resistant metal-nanoparticle-based catalysts. *Adv. Mater.* **2019**, *31*, 1901905.
(8) Wang, H.; Wang, L.; Xiao, F.-S. Metal@zeolite hybrid materials for catalysis. *ACS Cent. Sci.* **2020**, *6*, 1685−1697.
(9) Babucci, M.; Guntida, A.; Gates, B. C. Atomically dispersed metals on well-defined supports including zeolites and metal-organic frameworks: structure, bonding, reactivity, and catalysis. *Chem. Rev.* **2020**, *120*, 11956−11985.
(10) Liu, L.; Corma, A. Confining isolated atoms and clusters in crystalline porous materials for catalysis. *Nat. Rev. Mater.* **2021**, *6*, 244−263.
(11) Wang, Y.; Wang, C.; Wang, L.; Wang, L.; Xiao, F.-S. Zeolite fixed metal nanoparticles: new perspective in catalysis. *Acc. Chem. Res.* **2021**, *54*, 2579−2590.
(12) Deng, X.; Qin, B.; Liu, R.; Qin, X.; Dai, W.; Wu, G.; Guan, N.; Ma, D.; Li, L. Zeolite-encaged isolated platinum ions enable heterolytic dihydrogen activation and selective hydrogenations. *J. Am. Chem. Soc.* **2021**, *143*, 20898−20906.
(13) Knapp, C.; Obuchi, A.; Uchisawa, J. O.; Kushiyama, S.; Avila, P. Method for selective removal of supported platinum particles from external zeolite surfaces: characterisation of and application to a catalyst for the selective reduction of nitrogen oxide by hydrocarbons. *Microporous Mesoporous Mater.* **1999**, *31*, 23−31.
(14) Goel, S.; Zones, S. I.; Iglesia, E. Encapsulation of metal clusters within MFI via interzeolite transformations and direct hydrothermal syntheses and catalytic consequences of their confinement. *J. Am. Chem. Soc.* **2014**, *136*, 15280−15290.
(15) Mielby, J.; Abildstrøm, J. O.; Wang, F.; Kasama, T.; Weidenthaler, C.; Kegnæs, S. Oxidation of bioethanol using zeolite-encapsulated gold nanoparticles. *Angew. Chem., Int. Ed.* **2014**, *126*, 12721−12724.
(16) Wang, N.; Sun, Q.; Bai, R.; Li, X.; Guo, G.; Yu, J. In Situ Confinement of Ultrasmall Pd Clusters within Nanosized Silicalite-1 Zeolite for Highly Efficient Catalysis of Hydrogen Generation. *J. Am. Chem. Soc.* **2016**, *138*, 7484−7487.
(17) Wang, J.; Liu, L.; Dong, X.; Alfilfil, L.; Hsiung, C.-E.; Liu, Z.; Han, Y. Engineering of transition metal catalysts confined in zeolites. *Chem. Mater.* **2018**, *30*, 6361−6369.
(18) Cho, H. J.; Kim, D.; Li, J.; Su, D.; Xu, B. Zeolite-encapsulated Pt nanoparticles for tandem catalysis. *J. Am. Chem. Soc.* **2018**, *140*, 13514−13520.
(19) Iida, T.; Zanchet, D.; Ohara, K.; Wakihara, T.; Román-Leshkov, Y. Concerted bimetallic nanocluster synthesis and encapsulation via induced zeolite framework demetallation for shape and substrate selective heterogeneous catalysis. *Angew. Chem., Int. Ed.* **2018**, *57*, 6454−6458.
(20) Wang, L.; Xu, S.; He, S.; Xiao, F.-S. Rational construction of metal nanoparticles fixed in zeolite crystals as highly efficient heterogeneous catalysts. *Nanotoday* **2018**, *20*, 74−83.
(21) Zhang, J.; Wang, L.; Zhang, B.; Zhao, H.; Kolb, U.; Zhu, Y.; Liu, L.; Han, Y.; Wang, G.; Wang, C.; Su, D. S.; Gates, B. C.; Xiao, F.-S. Sinter-resistant metal nanoparticle catalysts achieved by immobilization within zeolite crystals via seed-directed growth. *Nat. Catal.* **2018**, *1*, 540−546.
(22) Chai, Y.; Liu, S.; Zhao, Z.-J.; Gong, J.; Dai, W.; Wu, G.; Guan, N.; Li, L. Selectivity modulation of encapsulated palladium nanoparticles by zeolite microenvironment for biomass catalytic upgrading. *ACS Catal.* **2018**, *8*, 8578−8589.
(23) Miyake, K.; Inoue, R.; Nakai, M.; Hirota, Y.; Uchida, Y.; Tanaka, S.; Miyamoto, M.; Nishiyama, N. Fabrication of Pt nanoparticles encapsulated in single crystal like silicalite-1 zeolite as a catalyst for shape-selective hydrogenation of C6 olefins. *Microporous Mesoporous Mater.* **2018**, *271*, 156−159.
(24) Pulikkal Thumbayil, R.; Mielby, J.; Kegnæs, S. Pd nanoparticles encapsulated in mesoporous HZSM-5 zeolite for selective one-step conversion of acetone to methyl isobutyl ketone. *Top. Catal.* **2019**, *62*, 678−688.
(25) Wang, N.; Sun, Q.; Yu, J. Ultrasmall metal nanoparticles confined within crystalline nanoporous materials: A fascinating class of nanocatalysts. *Adv. Mater.* **2019**, *31*, 1803966.
(26) Sun, Q.; Wang, N.; Bai, R.; Hui, Y.; Zhang, T.; Do, D. A.; Zhang, P.; Song, L.; Miao, S.; Yu, J. Synergetic effect of ultrasmall metal clusters and zeolites promoting hydrogen generation. *Adv. Sci.* **2019**, *6*, 1802350.
(27) Gao, X.; Zhou, Y.; Feng, L.; Tian, F.; Liu, X.; Xu, J.; Li, Y. Direct low-temperature hydrothermal synthesis of uniform Pd nanoparticles encapsulated mesoporous TS-1 and its excellent catalytic capability. *Microporous Mesoporous Mater.* **2019**, *283*, 82−87.
(28) Niu, R.; Liu, P.; Li, W.; Wang, S.; Li, J. High performance for oxidation of low-concentration methane using ultra-low Pd in silicalite-1 zeolite. *Microporous Mesoporous Mater.* **2019**, *284*, 235−240.
(29) Petrov, A. W.; Ferri, D.; Kröcher, O.; van Bokhoven, J. A. Design of stable palladium-based zeolite catalysts for complete methane oxidation by postsynthesis zeolite modification. *ACS Catal.* **2019**, *9*, 2303−2312.
(30) Shang, W.; Gao, M.; Chai, Y.; Wu, G.; Guan, N.; Li, L. Stabilizing isolated rhodium cations by MFI zeolite for heterogeneous methanol carbonylation. *ACS Catal.* **2021**, *11*, 7249−7256.
(31) Climent, M. J.; Corma, A.; Iborra, S.; Sabater, M. J. Heterogeneous catalysis for tandem reactions. *ACS Catal.* **2014**, *4*, 870−891.
(32) Cho, H. J.; Kim, D.; Li, S.; Su, D.; Ma, D.; Xu, B. Molecular-level proximity of metal and acid sites in zeolite-encapsulated Pt nanoparticles for selective multistep tandem catalysis. *ACS Catal.* **2020**, *10*, 3340−3348.
(33) Wu, Z.; Ge, S.; Ren, C.; Zhang, M.; Yip, A.; Xu, C. Selective conversion of cellulose into bulk chemicals over Brønsted acid promoted ruthenium catalyst: one-pot vs sequential process. *Green Chem.* **2012**, *14*, 3336−3343.
(34) Gutierrez-Acebo, E.; Leroux, C.; Chizallet, C.; Schuurman, Y.; Bouchy, C. Metal/acid bifunctional catalysis and intimacy criterion for ethylcyclohexane hydroconversion: when proximity does not matter. *ACS Catal.* **2018**, *8*, 6035−6046.
(35) Kay Lup, A. N.; Abnisa, F.; Daud, W. M. A. W.; Aroua, M. K. A review on reaction mechanisms of metal-catalyzed deoxygenation process in bio-oil model compounds. *Appl. Catal., A* **2017**, *541*, 87−106.
(36) Luo, W.; Cao, W.; Bruijnincx, P. C. A.; Lin, L.; Wang, A.; Zhang, T. Zeolite-supported metal catalysts for selective hydrodeoxygenation of biomass-derived platform molecules. *Green Chem.* **2019**, *21*, 3744−3768.
(37) Barrios, A. M.; Teles, C. A.; de Souza, P. M.; Rabelo-Neto, R. C.; Jacobs, G.; Davis, B. H.; Borges, L. E. P.; Noronha, F. B. Hydrodeoxygenation of phenol over niobia supported Pd catalyst. *Catal. Today* **2018**, *302*, 115−124.
(38) Kay Lup, A. N.; Abnisa, F.; Daud, W. M. A. W.; Aroua, M. K. Synergistic interaction of metal−acid sites for phenol hydrodeoxygenation over bifunctional Ag/TiO_2 nanocatalyst. *Chin. J. Chem. Eng.* **2019**, *27*, 349−361.
(39) Zhao, C.; He, J.; Lemonidou, A. A.; Li, X.; Lercher, J. A. Aqueous-phase hydrodeoxygenation of bio-derived phenols to cycloalkanes. *J. Catal.* **2011**, *280*, 8−16.
(40) Liu, Y.; Vjunov, A.; Shi, H.; Eckstein, S.; Camaioni, D. M.; Mei, D.; Baráth, E.; Lercher, J. A. Enhancing the catalytic activity of

https://doi.org/10.1021/acscatal.1c05012
ACS Catal. 2022, 12, 1847−1856

hydronium ions through constrained environments. *Nat. Commun.* **2017**, *8*, 14113−14121.
(41) de Souza, P. M.; Rabelo-Neto, R. C.; Borges, L. E. P.; Jacobs, G.; Davis, B. H.; Sooknoi, T.; Resasco, D. E.; Noronha, F. B. Role of keto intermediates in the hydrodeoxygenation of phenol over Pd on oxophilic supports. *ACS Catal.* **2015**, *5*, 1318−1329.
(42) de Souza, P. M.; Rabelo-Neto, R. C.; Borges, L. E. P.; Jacobs, G.; Davis, B. H.; Resasco, D. E.; Noronha, F. B. Hydrodeoxygenation of phenol over Pd catalysts. effect of support on reaction mechanism and catalyst deactivation. *ACS Catal.* **2017**, *7*, 2058−2073.
(43) Cho, H. J.; Xu, B. Enabling selective tandem reactions via catalyst architecture engineering. *Trends Chem.* **2020**, *2*, 929−941.
(44) Obenaus, U.; Dyballa, M.; Lang, S.; Scheibe, M.; Hunger, M. Generation and properties of Brønsted acid sites in bifunctional Rh-, Ir-, Pd-, and Pt-containing zeolites Y investigated by solid-state NMR spectroscopy. *J. Phys. Chem. C* **2015**, *119*, 15254−15262.
(45) Wu, Z.; Zhao, K.; Zhang, Y.; Pan, T.; Ge, S.; Ju, Y.; Li, T.; Dou, T. Synthesis and consequence of aggregated nanosized ZSM-5 zeolite crystals for methanol to propylene reaction. *Ind. Eng. Chem. Res.* **2019**, *58*, 10737−10749.
(46) Wu, Z.; Goel, S.; Choi, M.; Iglesia, E. Hydrothermal synthesis of LTA-encapsulated metal clusters and consequences for catalyst stability, reactivity, and selectivity. *J. Catal.* **2014**, *311*, 458−468.
(47) Liu, J.; Shi, W.; Ni, B.; Yang, Y.; Li, S.; Zhuang, J.; Wang, X. Incorporation of clusters within inorganic materials through their addition during nucleation steps. *Nat. Chem.* **2019**, *11*, 839−845.
(48) He, J.; Wu, Z.; Gu, Q.; Liu, Y.; Chu, S.; Chen, S.; Zhang, Y.; Yang, B.; Chen, T.; Wang, A.; Weckhuysen, B. M.; Zhang, T.; Luo, W. Zeolite-tailored active site proximity for the efficient production of pentanoic biofuels. *Angew. Chem., Int. Ed.* **2021**, *60*, 23713−23721.
(49) Pan, T.; Wu, Z.; Zhou, K. In situ incorporating Zn into hierarchical ZSM-5 zeolites for olefin hydroisomerization. *Ind. Eng. Chem. Res.* **2020**, *59*, 12371−12380.
(50) Woolery, G. L.; Alemany, L. B.; Dessau, R. M.; Chester, A. W. Spectroscopic evidence for the presence of internal silanols in highly siliceous ZSM-5. *Zeolites* **1986**, *6*, 14−16.
(51) Luo, W.; van Eck, E. R. H.; Bruijnincx, P. C. A.; Weckhuysen, B. M. Influence of levulinic acid hydrogenation on aluminum coordination in zeolite-supported ruthenium catalysts: A^{27}Al 3QMAS Nuclear Magnetic Resonance Study. *ChemPhysChem* **2018**, *19*, 379−385.
(52) Gilson, J.-P.; Edwards, G. C.; Peters, A. W.; Rajagopalan, K.; Wormsbecher, R. F.; Roberie, T. G.; Shatlock, M. P. Penta-co-ordinated aluminium in zeolites and aluminosilicates. *J. Chem. Soc., Chem. Commun.* **1987**, *2*, 91−92.
(53) Liu, J.; Hibbitts, D.; Iglesia, E. Dense CO adlayers as enablers of CO hydrogenation turnovers on Ru surfaces. *J. Am. Chem. Soc.* **2017**, *139*, 11789−11802.
(54) Zhang, W.; Chen, J.; Liu, R.; Wang, S.; Chen, L.; Li, K. Hydrodeoxygenation of lignin-derived phenolic monomers and dimers to alkane fuels over bifunctional zeolite-supported metal catalysts. *ACS Sustain. Chem. Eng.* **2014**, *2*, 683−691.
(55) Pfriem, N.; Hintermeier, P. H.; Eckstein, S.; Kim, S.; Liu, Q.; Shi, H.; Milakovic, L.; Liu, Y.; Haller, G. L.; Baráth, E.; Liu, Y.; Lercher, J. A. Role of the ionic environment in enhancing the activity of reacting molecules in zeolite pores. *Science* **2021**, *372*, 952−957.
(56) Zhang, C.; Jia, C.; Cao, Y.; Yao, Y.; Xie, S.; Zhang, S.; Lin, H. Water-assisted selective hydrodeoxygenation of phenol to benzene over the Ru composite catalyst in the biphasic process. *Green Chem.* **2019**, *21*, 1668−1679.

https://doi.org/10.1021/acscatal.1c05012
ACS Catal. 2022, 12, 1847−1856